Molecular Transport

Deutsche Ausgabe: DOI: 10.1002/ange.201908647
Internationale Ausgabe: DOI: 10.1002/anie.201908647

Selective Autonomous Molecular Transport and Collection by Hydrogel-Embedded Supramolecular Chemical Gradients

*Shiyan Zhang, Chunjie Zhang, Hao Chen, Spencer J. Kieffer, Frank Neubrech, Harald Giessen, Andrew G. Alleyne, and Paul V. Braun**

Abstract: *Selective transport and concentration of molecules to specified regions on a substrate both enhances the potential to detect such molecules and provides a path to spatially localize such molecules prior to initiation of subsequent chemical reactions. Here, we first embed radially symmetric α-, β-, and γ-cyclodextrin gradients in a hydrogel matrix. Driven by host-guest interactions between the cyclodextrins and the target molecule, we observe these gradients can serve to direct 2D molecular transport. Using xanthene dyes and organophosphates as target molecules, we found the transport metrics, e.g., selectivity, rate, and concentration limits, are strongly dependent on the specific cyclodextrin forming the gradient. In all cases, as the concentrating power of the gradient increased, the rate of target concentration slowed, which we hypothesize is because stronger interactions between the target and the cyclodextrin decrease the rate of target diffusion. The concentration enhancement for the nerve agent simulant 4-methylumbelliferyl phosphate (15.8) is the greatest when the gradient is formed using β-cyclodextrin while directed concentration of cyanomethyl phosphonate, a smaller non-aromatic organophosphate, is observed only for the smaller α-CD. To provide a near real-time read-out of the concentration of the analyte, we used an array of IR resonant metallic nanoantennas tuned to a specific IR absorption band of the analyte to enhance the IR signal generated by the analyte.*

The targeted transport and concentration of chemical and biological species to specified locations on surfaces has been suggested as an approach to enhance the detection limit of sensors constrained by diffusion-limited analyte collection.[1] Common methods to enhance analyte collection include pumped microfluidic systems[2] and application of electric or magnetic fields (for charged or magnetically-tagged analytes).[3] To enable autonomous molecular transport, approaches utilizing internal driving forces have been explored. Kinesin-based molecular motors have been shown to transport bonded cargos,[4] and surfaces containing chemical gradients have been used to transport DNA,[5] ions,[6] multivalent ligand molecules,[7] dendrimers,[8] poly(ethylene glycol),[9] but with the limitation that the system must be immersed in liquid to enable the transport. Recently, we reported the use of water-swollen (but not immersed in water) hydrogels films containing built-in charge or hydrophilicity gradients to transport and concentrate molecules.[10] However, the selectivity of the gradients in those cases were limited, as they only relied on charge or polarity to effect molecular transport.

Here, we embedded radially symmetric cyclodextrin (CD) gradients within hydrogel films and showed that these gradients can direct targeted molecules, including a model organophosphate, to concentrate within specific regions of the substrate via CD-target supramolecular interactions. Experiments and theory demonstrate that both the transport rate and molecular concentration enhancement is strongly correlated to the strength of the host-guest interaction, which is determined in-part by the cavity size. To provide a read-out of the concentration of the analyte, the CD gradient-containing hydrogel film was integrated with arrays of nanoantenna-based surface enhanced IR absorption (SEIRA)-based sensors.[11]

We embedded the radial cyclodextrin (CD)-based chemical gradient in a polyacrylamide (PAAm) hydrogel. This hydrogel chemistry was selected because its hydrophilicity makes it miscible with CD, its high water content speeds up the transport and concentration process, and it is relatively chemically inert (minimal interaction with the target molecules). The gradient was fabricated through spatially localized hydrolysis and amide coupling reactions (Figure 1). Following our previously report,[12] a few microliters of an alkaline hydrolysis solution was dosed on the center of a dry PAAm film resulting in a radially symmetric carboxylic acid gradient (the hydrolysis solution infuses into the hydrogel, hydrolyzing amide groups, forming a gradient of carboxylic acid groups). Then the carboxylic acid gradient was coupled with amine-appended α-, β-, γ-CD (Figure 1C) to construct the cyclodextrin gradients (see the Supporting Information (SI) for detailed experimental procedure). Note, the mesh size of the

[*] S. Zhang, C. Zhang, H. Chen, P. V. Braun
Department of Materials Science and Engineering, Beckman Institute for Advanced Science and Technology, and Materials Research Laboratory, University of Illinois at Urbana-Champaign
Urbana, Illinois 61801 (USA)
E-mail: pbraun@illinois.edu
F. Neubrech, H. Giessen
4th Physics Institute and Research Center SCoPE, University of Stuttgart, Pfaffenwaldring 57, 70569 Stuttgart (Germany)
F. Neubrech
Kirchhoff-Institute for Physics, University of Heidelberg
Im Neuenheimer Feld 227, 69120 Heidelberg (Germany)
S. J. Kieffer, A. G. Alleyne
Department of Mechanical Science and Engineering, University of Illinois at Urbana-Champaign, Urbana, Illinois 61801 (USA)
C. Zhang
Present address: 3M Company
3M Center, St. Paul, MN 55144 (USA)
Supporting information and the ORCID identification number(s) for the author(s) of this article can be found under https://doi.org/10.1002/anie.201908647.

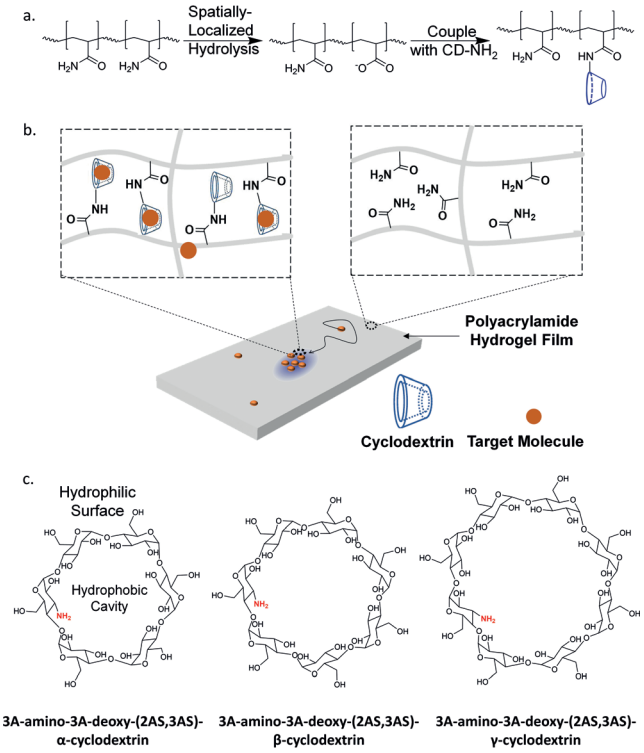

Figure 1. a) Gradient synthetic pathway formed via hydrolysis followed by coupling with amine-appended cyclodextrins. b) Schematic representation of the radial cyclodextrin chemical gradient in the PAAm hydrogel. Due to supramolecular interactions between cyclodextrins and target molecules, the target molecules are directed towards the center of the gradient. c) Chemical structure of 3A-amino-3A-deoxy-(2AS,3AS)-α-cyclodextrin, 3A-amino-3A-deoxy-(2AS,3AS)-β-cyclodextrin, and 3A-amino-3A-deoxy-(2AS,3AS)-γ-cyclodextrin.

hydrogel (4.2 nm) is significantly greater than the largest dimension of the CDs (≈0.8 nm), so we expect the CD to fully penetrate the hydrogel film during synthesis of the gradient.[13]

We hypothesize that once the targeted molecules reach the CD gradient, they will be selectively concentrated if they form reversible guest-host complexes with the CDs. The target transport in the CD gradient region consists of three processes: diffusion through the PAAm hydrogel, association with CD, and disassociation from CD (Figure 2). As long as the target molecule has only weak interactions with the PAAm hydrogel, it will diffuse relatively freely before approaching a polymer conjugated CD. Once it encounters a CD, the target molecule can enter the CD cavity for a period of time slowing its rate of diffusion. The formation of the host–guest complex between target molecules and CD is a reversible process driven by non-covalent interactions that can be described by the binding constant K. K is affected by the size-match of the target molecule with the size of the CD cavity, the water solubility of target molecules, and the conformation of target molecules.[14] For example, non-aromatic chains usually associate more strongly with the relatively small cavities of α-CD, while the larger phenyl and heterocyclic groups match better with the larger cavities of β- and γ-CD.

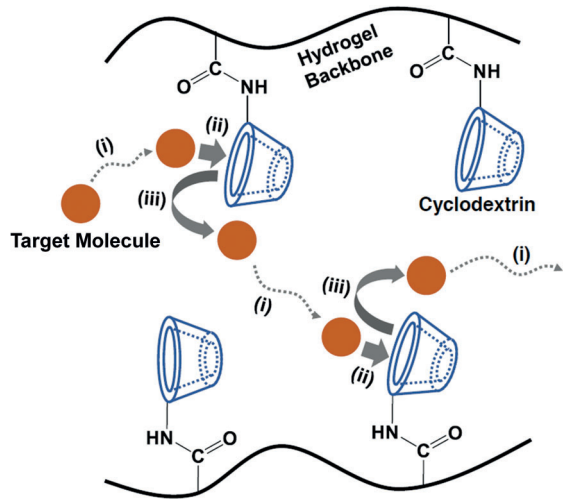

Figure 2. Schematic illustration of a target molecule diffusing inside a cyclodextrin-conjugated hydrogel: (i) diffusion through the hydrogel, (ii) association with cyclodextrin and (iii) dissociation of the inclusion complex.

We selected xanthene dyes as model compounds to visualize the directed molecular transport process within CD gradients. After dosing two dye spots (0.1 μL each of 0.2 mM dye in pH 7.4 PBS) outside of the gradient ca. 4 mm from the gradient center (Figure 3a), the fluorescence was monitored over time in a 100% relative humidity environment (Figure 3b–e). To study the influence of the guest chemical structure, the transport of fluorescein and rhodamine B (Rh B), which have different substituents on xanthene

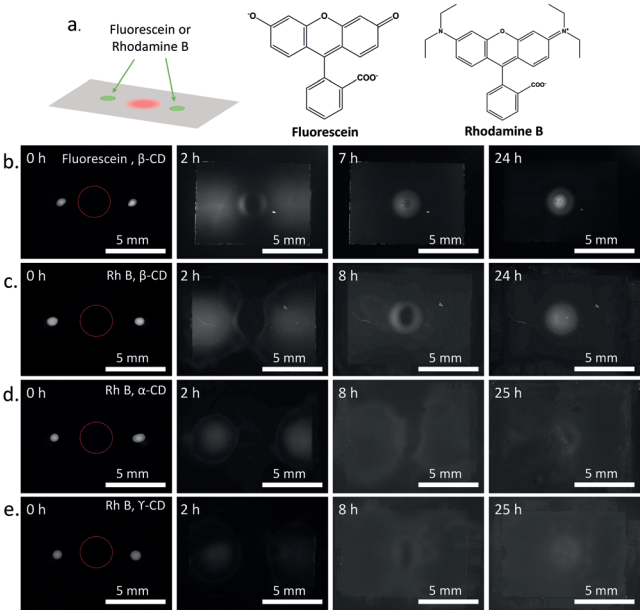

Figure 3. Directed concentration process of xanthene-based fluorescent dyes in radial α-, β-, and γ- cyclodextrin gradients. a) Sample schematic and dye chemical structures. b,c) With the β-cyclodextrin gradient, Fl (b) concentrates faster than Rh B (c). c,d,e) For the same dye (Rh B), c) β-, d) α- and e) γ-cyclodextrin gradients drive different concentration enhancements, indicating that the cyclodextrin cavity size impacted gradient-directed dye concentration.

but the same carboxyphenyl group (Figure 3a), were studied on the same radially symmetric β-CD gradient (Figure 3b,c). Initially, both fluorescein and Rh B diffused freely into the hydrogel surrounding the dosing spots. 2 h following dosing, both Rh B and fluorescein have reached the β-CD gradient, and started to accumulate at the rim of the gradient (more so in the case of fluorescein). After 7 to 8 h, Rh B is still accumulating at the gradient rim and only slowly moving towards the center of the gradient, while fluorescein has already reached the gradient center. By 24 h, both fluorescein and Rh B have reached the gradient center, with fluorescein appearing to be more concentrated at the center than Rh B. As the quantity of dye dosed on the substrate (0.04 μmol) exceeds the quantity of OH- used for hydrolysis (0.03 μmol), even if the hydrolysis yield is unity, all hydrolyzed groups are conjugated with cyclodextrins, and all cyclodextrins form the host–guest complexes with the dyes, based on the ratio of the total area of the substrate and the area of the gradient, the maximum concentration enhancement will be ≈ 70. However, due to potential effects such as fluorescence quenching, we do not attempt to extract quantitative dye concentrations vs. time from the fluorescent images and save such analysis for the Raman-based studies.

Both fluorescein and Rh B can form inclusion complexes with β-CD via interactions of the xanthene or carboxyphenyl groups with the CD cavity,[15] with the reported binding constant K of Rh B–β-CD greater than that of fluorescein–β-CD.[16] Based on our observation that Rh B appears to move more slowly in the β-CD gradient, we suggest that the Rh B molecules have stronger interactions with β-CD than fluorescein, perhaps due to Rh B's N,N-diethyl substituents. This assumption is supported by the diffusion studies of fluorescein and Rh B in a homogeneously β-CD conjugated PAAm hydrogel. In this conjugated hydrogel, $D = 0.19 \pm 0.05 \times 10^{-6}$ for Fluorescein and $D = 0.11 \pm 0.02 \times 10^{-6}\,cm^2 s^{-1}$ for Rh B (see SI for detailed experimental procedure and calculation), indicating Rh B binds more strongly with β-CDs than fluorescein.

On α- and γ-CD gradients, the directed concentration of Rh B was less obvious (Figure 3d,e). The diffusion coefficients of Rh B in α- ($D = 0.18 \pm 0.26 \times 10^{-6}\,cm^2 s^{-1}$) and γ-CD ($D = 0.48 \pm 0.08 \times 10^{-6}\,cm^2 s^{-1}$) conjugated PAAm hydrogel are much greater than in the β-CD conjugated hydrogel, (see SI for detailed experimental procedure and calculation). This agrees with literature reports that Rh B associates strongly with β-CD but only weakly with α- and γ-CD.[17] We suggest it is the weaker association between Rh B and α- or γ-CD that makes the directed transport of Rh B in those systems less apparent.

The spatial and temporal concentration of the target molecule was quantified using confocal Raman spectroscopy during the directed molecular transport (Figure 4). As the target molecule, we selected 4-methylumbelliferyl phosphate (MUP), a model organophosphate with a signature Raman peak at 1558 cm^{-1} provided by its aromatic ring structure (CDs have gained attention for their potential for the detection of toxic organophosphate[18]). The gradient diameter is around 1 mm, formed as we previously described.[12] Initially several spots of a 10 mM MUP solution (0.8 μL each spot) were dosed outside of the α-, β- or γ-CD gradient on the hydrogel in a row (Figure 4a, SI Figure 3). Then, similar to the fluorescence transport studies, samples were placed in a 100% relative humidity chamber to swell the hydrogel and initiate transport. Following the initiation of transport, Raman spectra are scanned across the gradient at different times. All Raman spectra were normalized by the peak at ca. 1100 cm^{-1} corresponding to the C–C stretching of the PAAm backbone. The directed transport and concentration of MUP was observed on all α-, β-, and γ-CD gradient embedded hydrogel samples. At the initial dosing position, the peak intensity at ca. 1558 cm^{-1} is highest at $t = 1$ h and continuously decreases with time due to free diffusion until MUP is distributed nearly homogeneously outside the gradient (Figure 4b–d, SI Figure 3b–d). At a distance of 2 mm from the gradient center, the peak intensity first slightly increases as MUP diffuses into that region (Figure 4e–g, SI Figure 3e–g), and then stays about the same or decreases. At the gradient center, the initial MUP concentration is zero, and over time increases to be higher than even the intensity at the initial dosing position at the beginning (Figure 4h-m, SI Figure 3h–m).

Although directed transport and concentration of MUP was observed on α-, β-, and γ-CD gradient containing hydrogels, the degree of concentration of MUP depends on the CD cavity size. We quantify the directed concentration capability of different CD gradients using the concentration enhancement ratio (CER), which is the ratio of the averaged MUP signal intensity in the gradient center region (−0.4 mm to 0.4 mm) to the averaged MUP signal intensity outside the gradient (= ± 2 to 8 mm). The CER after 40 h of transport follows the same sequence over the investigated range of MUP dosing concentrations: $CER_{\beta\text{-CD}}(15.8) > CER_{\gamma\text{-CD}}(9.4) > CER_{\alpha\text{-CD}}(7.8)$ (Figure 4k–m, SI Figure 3k–m). By integrating the Raman intensity over the sample, we determine that while the gradient center region accounts for only ≈ 0.3% of the sample area, it accumulates 2.3%, 4.4%, 2.8% of the MUP target when derivatized with α-, β-, and γ-CDs, respectively. The MUP diffusion coefficients on α-, β-, and γ-CD modified PAAm hydrogels follow the sequence of interaction strengths: $D_{\beta\text{-CD}}(0.52 \pm 0.14 \times 10^{-6}\,cm^2 s^{-1}) < D_{\gamma\text{-CD}}(0.65 \pm 0.19 \times 10^{-6}\,cm^2 s^{-1}) < D_{\alpha\text{-CD}}(1.01 \pm 0.18 \times 10^{-6}\,cm^2 s^{-1})$. A phenomenon caused by the low MUP diffusion coefficient on β-CD conjugated hydrogel is that after 21 h of MUP transport in a β-CD gradient containing hydrogels, the MUP signal intensity is slightly greater in the periphery region of the gradient than in the center of the gradient over a range of initial MUP dosings (Figure 4I, SI Figure 3I). Building off previous work[19] we suggest the relatively large aromatic ring structure of MUP is a closer match to the β- and γ-CD cavity sizes than the α-CD cavity size, and thus the reason for MUP's stronger interactions with these CDs than with α-CD. On the contrary, directed concentration of cyanomethyl phosphonate (CDNMP), a relatively smaller non-aromatic organophosphate, is observed only for the smaller α-CD (SI Figure 4).

Following to our previous study,[10b] the concentration $C(x,y)$ distribution of target molecules in a chemical gradient can be described by the diffusion-convection equation,

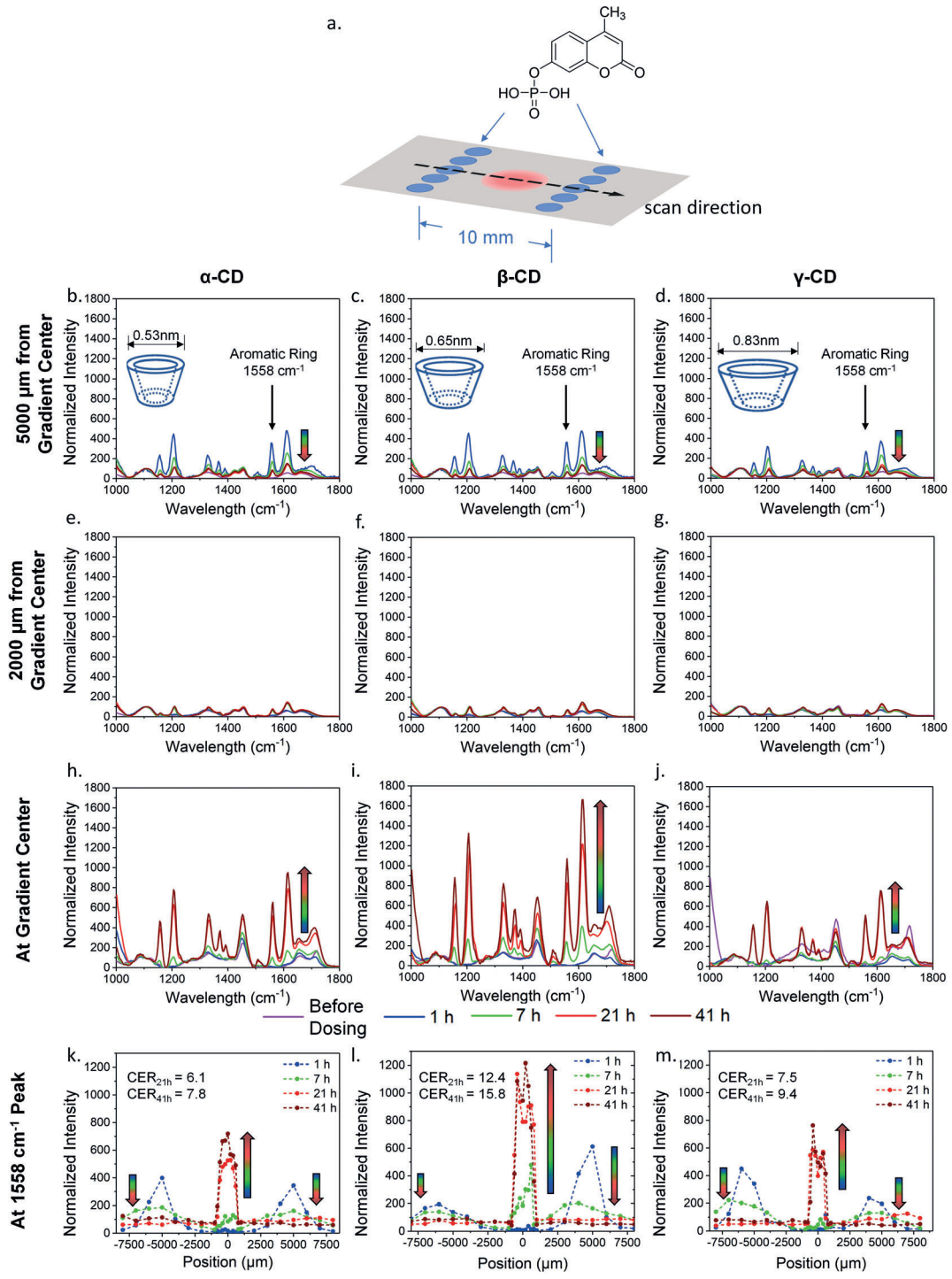

Figure 4. Raman-based quantification of directed concentration of 4-methylumbelliferyl phosphate (MUP) in radial α-, β-, and γ-cyclodextrin gradients. a) Experimental schematic. Initially, 10 spots of MUP solution (0.8 µL, 10 mM) are dosed outside the gradient in a row 5 mm (nearest distance) from the gradient center. Raman spectra are collected along the dotted line at increasing times. b–j) Normalized Raman spectra at different times and the indicated distance from the gradient center. b–d) at the dosing point (5000 µm from the gradient center), e–g) 2000 µm from the gradient center, and h–j) at the gradient center for α-, β-, and γ- cyclodextrin gradients. The 1558 cm^{-1} peak corresponding to the aromatic ring of MUP is used to determine the MUP concentration distribution in the hydrogel. "Before Dosing" spectra are before dosing the MUP solution. k–m) Plots of the normalized 1558 cm^{-1} peak intensity as a function of position and time. CER is the concentration enhancement ratio, see text for details.

$\frac{\partial C}{\partial t} = -\nabla[D\nabla C] - \nabla[\nu C]$, in which $D(x,y)$ and $\nu(x,y)$ are the local diffusion constant and the drift velocity induced by the chemical gradient. In this study, given the same gradient geometric parameters and functional binding site density distribution $\rho(x,y)$, $D(x,y)$ will be exponentially related to the binding site energy ε,[20]

$$D = \alpha \exp\left(-\frac{\beta\rho\varepsilon}{k_B T}\right), \quad (1)$$

where α,β are parameters that are determined by the gradient geometry and the PAAm substrate property, k_B is the Boltzmann constant, and T is the temperatur. The drift velocity $v(x,y)$, is proportional to $D(x,y)$, ε, and $\nabla\rho(x,y)$. Here we assume the same $\rho(x,y)$ and thus the same $\nabla\rho(x,y)$ for all experiments, so $v(x,y)$ can be desribed as

$$v = \frac{\lambda D\varepsilon}{k_B T}\nabla\rho = \frac{\alpha\lambda\varepsilon}{k_B T}\exp\left(-\frac{\beta\rho\varepsilon}{k_B T}\right), \quad (2)$$

where λ is a constant determined by the gradient geometry. For a detailed discussion, we refer the reader to Refs. [1a] and [20]. Note there may be a distribution of binding site energies (e.g. both due to binding of the analyte to CDs and to the host hydrogel matrix), and all possible binding sites must be included in the analysis.

Considering the above analysis, it is clear that to achieve the optimal directed molecular transport rate in the gradient region, ε must fall in the appropriate range. If ε is too large, molecules may accumulate at the gradient edge for a long time since D becomes very small towards the gradient center as ρ increases. This can possibly explain the higher MUP concentration in the peripheral β-CD gradient region. In the limit of large ε, molecules would simply permanently bind at the gradient edge. Although a higher ε in the gradient region may slow down the transport rate by decreasing D in the gradient region, given sufficient time, it will enhance the molecular concentration capability of the gradient as demonstrated quantitatively by the MUP transport results on the different CD gradients. As can be observed from the transport results of Rh B on α- and γ-CD gradients, if ε is too low, molecular concentration will be limited.

To demonstrate the potential of integrating radially distributed CD-gradient embedded hydrogel films with resonant sensors, we coated the hydrogel film on a surface patterned with a surface enhanced IR absorption (SEIRA) nanoantenna sensor. The function of the SEIRA sensor is to selectively enhance the IR absorbance of the vibrational mode of interest.[11,21] Here SEIRA is used to enhance IR-active organophosphate vibrational modes, e.g., P-O-C and P=O stretches, to demonstrate the potential for sensing of toxic organophosphate. In our integrated device, a 300 μm × 300 μm patch of 3 μm × 80 nm × 50 nm SEIRA-active nanoantennas were fabricated on a 1 × 1 cm^2 CaF_2 substrate, then coated with a β-CD gradient containing hydrogel. The gradient center was aligned with the nanoantennas such that target molecules would be concentrated over the sensing area (Figure 5a). The MUP was selected as the target molecule and initially dosed on the hydrogel in two opposite lines 3.5 mm at closest approach to the gradient center (10 mM, 3 spots on each line, 0.8 μL each spot). During the directed transport and concentration in a 100% relative humidity environment, IR absorption spectra were taken at the center of the nanoantenna patch at selected time points. As shown in Figure 5c, the peak intensity at ca. 1095 cm^{-1}, which corresponds to the P=O stretching, increases continuously as

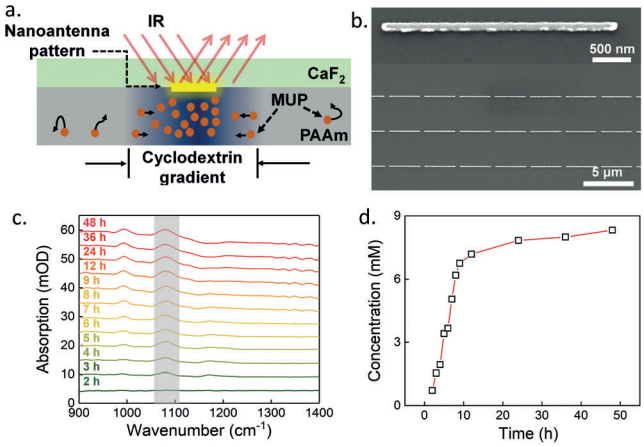

Figure 5. CD gradient containing hydrogel coating on a SEIRA sensor. a) Schematic representation of the SEIRA sensor, and the hydrogel containing the embedded cyclodextrin gradient. b) SEM of the array of gold nanoantennas providing SEIRA. c) Absorption spectra at the gradient center over time as a β-CD gradient directs the transport of MUP. d) Concentration of MUP over time in nanoantenna sensing area calculated from the integrated absorbance of the P=O stretching vibration at ca. 1095 cm^{-1}.

transport proceeds. Since the P=O stretch intensity is linearly related to the MUP concentration in the sensing area (SI Figure 5), we can quantify the local MUP concentration as a function of time from IR spectra. As illustrated in Figure 5d, the MUP concentration increases sharply from 0.7 mM at 1 h to 6.9 mM at 10 h, then increases gradually reaching 8.4 mM after 50 h.

In summary, we show that hydrogels containing embedded radially distributed CD gradients enable the selective molecular transport and concentration of various compounds, including organophosphates, and that CD cavity size can be used to tune transport and concentration behaviors. Control of the interaction strength between the target molecules and CDs, which can be represented by the binding energy or binding constant, both modulate the overall transport rate and determine the ultimate concentration enhancement. Using MUP as a model transport molecule, the cyclodextrin gradient embedded PAAm hydrogel can provide a 15.8 fold concentration enhancement. By integrating a chemical gradient with an embedded SEIRA nanoantenna sensor, we are able to detect these model compounds using a general approach applicable for a range of applications.

Acknowledgements

The work was supported by the Defense Threat Reduction Agency under award number HDTRA 1-12-1-0035, the Department of Defense/US Army W911NF-17-1-0351, the Alexander von Humboldt foundation (Bessel prize to P.V.B.), MWK BW (Spitzenforschung II), DFG, BMBF, ERC (ComplexPlas), and the Zeiss Foundation. We thank Dr. Brian Pate (DTRA), Dr. Tsung-Han Tsai, Dr. Mohammad Amdad Ali, Dr. Kali Miller, Dr. Dianwen Zhang, and Zheng Chen (Yale) for helpful discussions, technical advice and support.

Conflict of interest

The authors declare no conflict of interest.

Keywords: chemical gradient · cyclodextrin · molecular transport · selectivity · supramolecular interaction

[1] a) A. Sitt, H. Hess, *Nano Lett.* **2015**, *15*, 3341 – 3350; b) S. Das, O. E. Shklyaev, A. Altemose, H. Shum, I. Ortiz-Rivera, L. Valdez, T. E. Mallouk, A. C. Balazs, A. Sen, *Nat. Commun.* **2017**, *8*, 14384; c) V. Rodriguez-Ruiz, A. Maksimenko, G. Salzano, M. Lampropoulou, Y. G. Lazarou, V. Agostoni, P. Couvreur, R. Gref, K. Yannakopoulou, *Sci. Rep.* **2017**, *7*, 835.

[2] P. Marmottant, S. Hilgenfeldt, *Proc. Natl. Acad. Sci. USA* **2004**, *101*, 9523 – 9527.

[3] a) N. Islam, J. Wu in *International Mems Conference 2006*, *Vol. 34*, **2006**, pp. 356 – 361; b) S. Sanchez, A. A. Solovev, S. M. Harazim, O. G. Schmidt, *J. Am. Chem. Soc.* **2011**, *133*, 701 – 703.

[4] a) G. D. Bachand, S. B. Rivera, A. Carroll-Portillo, H. Hess, M. Bachand, *Small* **2006**, *2*, 381 – 385; b) E. R. Kay, D. A. Leigh, F. Zerbetto, *Angew. Chem. Int. Ed.* **2007**, *46*, 72 – 191; *Angew. Chem.* **2007**, *119*, 72 – 196; c) J. Bath, A. J. Turberfield, *Nat. Nanotechnol.* **2007**, *2*, 275 – 284.

[5] B. Maier, J. O. Radler, *Phys. Rev. Lett.* **1999**, *82*, 1911 – 1914.

[6] C. Reznik, Q. Darugar, A. Wheat, T. Fulghum, R. C. Advincula, C. F. Landes, *J. Phys. Chem. B* **2008**, *112*, 10890 – 10897.

[7] A. Perl, A. Gomez-Casado, D. Thompson, H. H. Dam, P. Jonkheijm, D. N. Reinhoudt, J. Huskens, *Nat. Chem.* **2011**, *3*, 317 – 322.

[8] T. Chang, D. I. Rozkiewicz, B. J. Ravoo, E. W. Meijer, D. N. Reinhoudt, *Nano Lett.* **2007**, *7*, 978 – 980.

[9] P. Burgos, Z. Y. Zhang, R. Golestanian, G. J. Leggett, M. Geoghegan, *ACS Nano* **2009**, *3*, 3235 – 3243.

[10] a) T. H. Tsai, M. A. Ali, Z. L. Jiang, P. V. Braun, *Angew. Chem. Int. Ed.* **2017**, *56*, 5001 – 5006; *Angew. Chem.* **2017**, *129*, 5083 – 5088; b) C. J. Zhang, A. Sitt, H. J. Koo, K. V. Waynant, H. Hess, B. D. Pate, P. V. Braun, *J. Am. Chem. Soc.* **2015**, *137*, 5066 – 5073.

[11] a) R. Adato, S. Aksu, H. Altug, *Mater. Today* **2015**, *18*, 436 – 446; b) F. Neubrech, C. Huck, K. Weber, A. Pucci, H. Giessen, *Chem. Rev.* **2017**, *117*, 5110 – 5145.

[12] S. Y. Zhang, S. J. Kieffer, C. J. Zhang, A. G. Alleyne, P. V. Braun, *Adv. Mater.* **2018**, *30*, 0.

[13] "Functionalized hydrogel systems for molecular sensing and transport": C. Zhang, PhD Dissertation, University of Illinois at Urbana-Champaign, **2015**.

[14] a) M. R. Eftink, M. L. Andy, K. Bystrom, H. D. Perlmutter, D. S. Kristol, *J. Am. Chem. Soc.* **1989**, *111*, 6765 – 6772; b) A. Harada, Y. Takashima, H. Yamaguchi, *Chem. Soc. Rev.* **2009**, *38*, 875 – 882; c) J. X. Zhang, P. X. Ma, *Adv. Drug Delivery Rev.* **2013**, *65*, 1215 – 1233; d) E. M. M. Del Valle, *Process Biochem.* **2004**, *39*, 1033 – 1046; e) X. L. Luan, Y. H. Zhang, J. Wu, P. Jonkheijm, G. T. Li, L. Jiang, J. Huskens, Q. An, *ChemistryOpen* **2016**, *5*, 331 – 338.

[15] L. N. Bogdanova, N. O. McHedlov-Petrossyan, N. A. Vodolazkaya, A. V. Lebed, *Carbohydr. Res.* **2010**, *345*, 1882 – 1890.

[16] a) L. Flamigni, *J. Phys. Chem.* **1993**, *97*, 9566 – 9572; b) Y. Degani, I. Willner, Y. Haas, *Chem. Phys. Lett.* **1984**, *104*, 496 – 499.

[17] S. F. Lincoln, J. H. Coates, R. L. Schiller, *J. Inclusion Phenomena* **1987**, *5*, 709 – 716.

[18] S. Letort, S. Balieu, W. Erb, G. Gouhier, F. Estour, *Beilstein J. Org. Chem.* **2016**, *12*, 204 – 228.

[19] S. Letort, S. Balieu, W. Erb, G. Gouhier, F. Estour, *Beilstein J. Org. Chem.* **2016**, *12*, 204 – 228.

[20] K. Oura, V. G. Lifshits, A. Saranin, A. V. Zotov, M. Katayama, *Surf. Sci.* **2003**, 325 – 356.

[21] B. Luk'yanchuk, N. I. Zheludev, S. A. Maier, N. J. Halas, P. Nordlander, H. Giessen, C. T. Chong, *Nat. Mater.* **2010**, *9*, 707 – 715.

Manuscript received: July 11, 2019
Revised manuscript received: August 27, 2019
Accepted manuscript online: September 22, 2019
Version of record online: ■■ ■■, ■■■■

Zuschriften

Molekültransport

S. Zhang, C. Zhang, H. Chen, S. J. Kieffer, F. Neubrech, H. Giessen, A. G. Alleyne, P. V. Braun* ——— ■■■■–■■■■

Selective Autonomous Molecular Transport and Collection by Hydrogel-Embedded Supramolecular Chemical Gradients

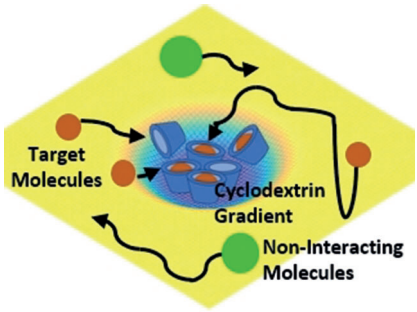

Ein Hydrogelfilm mit eingebautem radialsymmetrischem Cyclodextrin-Gradienten ist zum selektiven Molekültransport befähigt. Die Transporteigenschaften, einschließlich der Selektivität, Geschwindigkeit und Konzentrationsgrenze, hängen von der Stärke der Wirt-Gast-Wechselwirkung ab. Mit einer Anordnung von IR-resonanten Nanosensoren konnte die Konzentration eines Analyten quantifiziert werden.